J Electroceram (2007) 18:161–165
DOI 10.1007/s10832-007-9019-4

Study of PEDOT:PSS-SnO_2 nanocomposite film as an anode for polymer electronics

Seok-Joo Wang · Hyung-Ho Park

Received: 27 June 2005 / Accepted: 18 October 2006 / Published online: 22 February 2007

Abstract Poly(3,4-ethylenedioxythiophene) oxidized with poly(4-styrenesulfonate)(PEDOT:PSS) is a candidate material for applications in molecular electronics, such as organic field effect devices, organic photovoltaics, and organic light emitting devices. The properties of 3.5–4.0 nm sized SnO_2 nanoparticles doped PEDOT:PSS films were investigated for anode application. Sheet resistance was decreased and rms roughness was slightly increased with the incorporation of SnO_2 nanoparticles. However, the connectivity of conducting grains was improved by the plasticizing effect of surface –OH groups of SnO_2 nanoparticle. Using photoemission spectroscopy and near edge X-ray absorption fine structure (NEXAFS), the electronic structure of the films is studied comparatively on the C 1*s* NEXAFS, secondary electron emission cut off, and valence band spectra. The start of electron emission retarded and valence band maximum was increased in the PEDOT:PSS-SnO_2 nanocomposite films. These changes in the electronic structure resulted from emitted electron screening of core-hole in the PEDOT:PSS energy band and electron donation of SnO_2 nanoparticles.

Keywords PEDOT:PSS · SnO_2 · Nanoparticle · PES · NEXAFS

1 Introduction

Polymer electronics is considered as a promising technology for large, flexible, lightweight, and flat-panel displays. Such devices consist of one or several semiconducting organic layer(s) sandwiched between two electrodes. In this field, organic–inorganic hybrid materials are media for electronic and optoelectronic applications. Thin films of an electrically conducting polymer blend, poly(3,4-ethylenedioxythiophene) oxidized with poly(4-styrenesulfonate)(PEDOT:PSS) layers improve the injection of holes in organic light emitting devices (OLED) and can replace commonly used material (indium tin oxide: ITO) in case of flexible display and also these injection layers show favorable work function. It shows many advantages over other conducting polymers, such as a high transparency in the visible range, excellent thermal stability, and it can be processed in aqueous solution. However, commercially available PEDOT:PSS can be easily spin-coated and resulted in highly transparent and conducting (0.05–10 Vs/cm) polymer films. To use this polymer as an anode material in flexible devices, high conductivity and good mechanical, thermal, and environmental stabilities are needed [1, 2]. Conductivity enhancement has been studied by adding secondary dopant, such as DMSO, THF, Sorbitol, EG, etc., by many researchers [2–4].

In this article, we studied the roles of SnO_2 nanoparticles in PEDOT:PSS film. The combination of nanosized inorganic components with organic polymers endows the resulted nanocomposite with good processability and improved physical, mechanical, and electrical properties such as enhanced solubility, conductivity, and optoelectronic properties, etc., which has drawn considerable attention recently. The secondary doping of PEDOT:PSS with SnO_2 nanoparticle was interpreted in terms of morphology changes, surface bonding states, and electron emission energies by using atomic force microscopy (AFM), photoemission spectroscopy (PES), and near edge X-ray absorption fine structure (NEXAFS).

S.-J. Wang · H.-H. Park (✉)
Department of Ceramic Engineering, Yonsei University,
Seoul 120-749, South Korea
e-mail: hhpark@yonsei.ac.kr

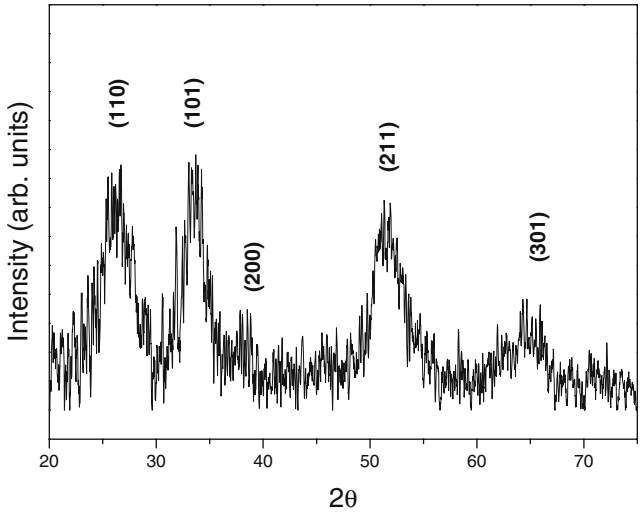

Fig. 1 XRD pattern for SnO_2 particles calcined at 400°C

2 Experimental procedure

SnO_2 nanoparticles were successfully prepared by means of dissolving of tin chloride (hydrous $SnCl_4 \cdot 5H_2O$) in distilled water. In a typical synthesis, an aqueous ammonia solution was added to the above solution. Heat treatment of the synthesized SnO_2 nanoparticles was conducted at 400°C. Conductive PEDOT:PSS and PEDOT:PSS-SnO_2 nanocomposite films were formed by spin casting of commercial aqueous PEDOT:PSS solution (Baytron P, AI 4073) on glass substrate (Corning 1737) with a speed of 400 rpm. The addition of IPA was 1:1 in v/o and SnO_2 was 25 and 50 w/o with respect to the PEDOT:PSS solution. The PEDOT:PSS-SnO_2 nanocomposite films were dried at 80 and 120°C for 5 min each to remove IPA and H_2O, and finally annealed at 200°C for 10 min. X-ray diffraction (XRD) pattern of SnO_2 nanoparticles was acquired by using a Rigaku XRD system (Fe $K\alpha$-radiation) and AFM images were taken by using Dimension 3100 instrument (Digital instruments) set at tapping and phase mode. Sheet resistance of the films was measured using a four-point probe technique. In order to investigate the chemical bonding states, secondary edge emission, and C 1*s* K-edge absorption of PEDOT:PSS-SnO_2 composite films as a function of nanoparticle addition by synchrotron radiation photoemission spectroscopy (SRPES), were loaded into a vacuum chamber, equipped with an electron analyzer, in the 4B1 beam line at the Pohang Accelerator Laboratory (PAL). The incident photon energy of 350 eV was used to obtain spectra. The onset of photoemission, corresponding to the vacuum level at the surface of sample was measured with negative bias (−20 V) on the sample to avoid work function of the detector. The incident photon energy was calibrated with the core level spectrum of Au 4*f*.

3 Results and discussion

Nanoscale SnO_2 nanoparticles were fabricated by the conventional method in elsewhere [5]. In Fig. 1, XRD pattern is given for the as-prepared SnO_2 nanoparticles annealed at 400°C for 2 h. All the diffraction lines are assigned to the rutile structure with tetragonal system of tin oxide. The average nanoparticle size (t) was calculated at ca. 3.5–4.0 nm using the Scherrer equation [6]. SnO_2 nanoparticles synthesized from aqueous solution usually have surface −OH groups. SnO_2 is n-type semiconductor with oxygen vacancies or interstitial Sn atoms naturally and it is important on the nanoparticle surface [7].

PEDOT:PSS-SnO_2 nanocomposite film showed decreased surface sheet resistance with the increase in the concentration of SnO_2 nanoparticles. Sheet resistances of PEDOT:PSS, PEDOT:PSS-SnO_2 (25%), PEDOT:PSS SnO_2 (50%) films are 4.6, 1.8, and 1.5 kΩ/□, respectively. By addition of SnO_2 nanoparticle, surface resistance was decreased to ca. one-third of PEDOT:PSS film. X-ray photoelectron spectroscopy (XPS) analysis was conducted to understand the change in the bonding states of PEDOT:PSS by the incorporation of SnO_2 nanoparticles. In Fig. 2,

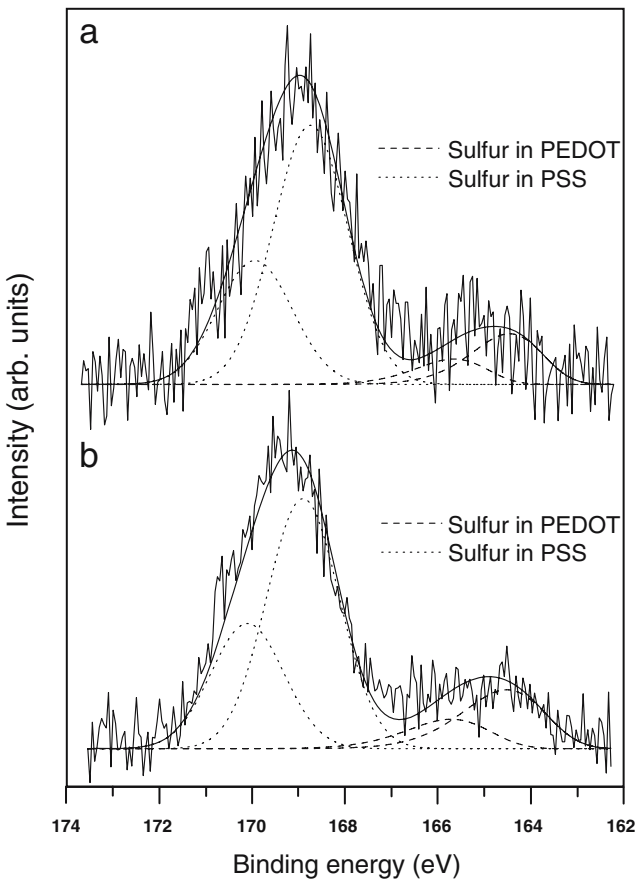

Fig. 2 S 2*p* core level spectra of **a** PEDOT:PSS-SnO_2(25%) and **b** PEDOT-PSS

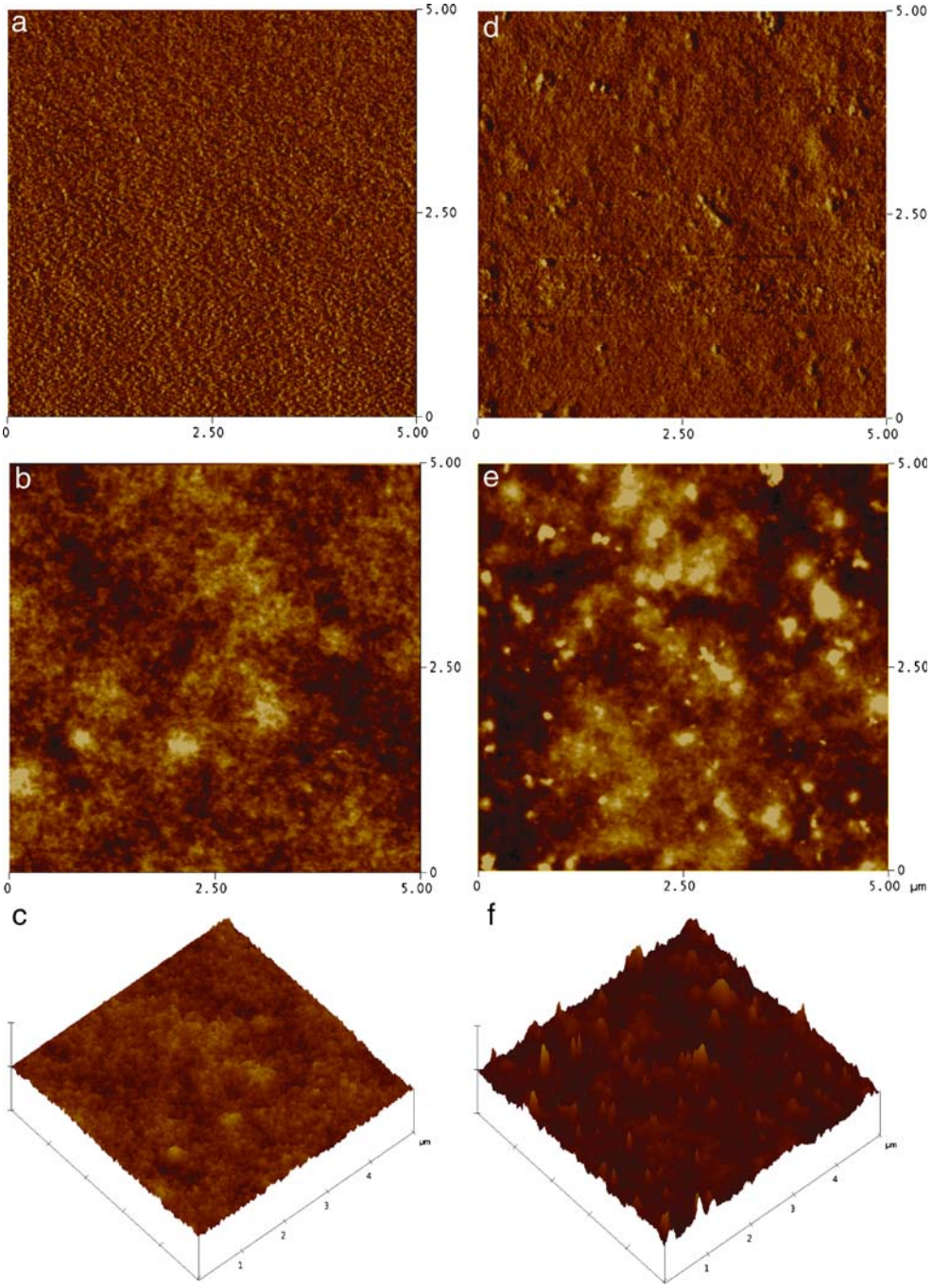

Fig. 3 AFM images of **a**/**d** phase, **b**/**e** height, and **c**/**f** 3-D representation of PEDOT:PSS and PEDOT:PSS-SnO_2 (25%) nanocomposite films, respectively

S 2*p* core level feature of PEDOT:PSS shows S bonds in PEDOT and PSS separately [4, 8]. Bonding area of S bonds in PEDOT increased somewhat from 16.6 to 21.7% after the incorporation of SnO_2. The values of full width at half maximum were also increased by 0.3 and 0.1 both in S bonds in PEDOT and PSS, respectively. This suggests that the improvement in conductivity (decrease in sheet resistance) is in some part due to the chemical changes in the film surface. SnO_2 nanoparticles seemed to incorporate into PEDOT:PSS and weaken the electrostatic interaction.

In Fig. 3, AFM images of PEDOT:PSS and PEDOT:PSS-SnO_2 (25%) films were given. The topography of the films slightly changed and rms roughness value increased from 1.661 to 3.562 nm with PEDOT:PSS-SnO_2 (25%) film by appearing some large domains. The presence of inorganic SnO_2 nanoparticle increases the rms value due to its size factor and the tendency of agglomeration. **c** and **f** correspond to three-dim. surface topographic images of height images, **b** and **e**. In phase mode images, **a** and **d**, the connectivity of grains was found to be improved. Phase

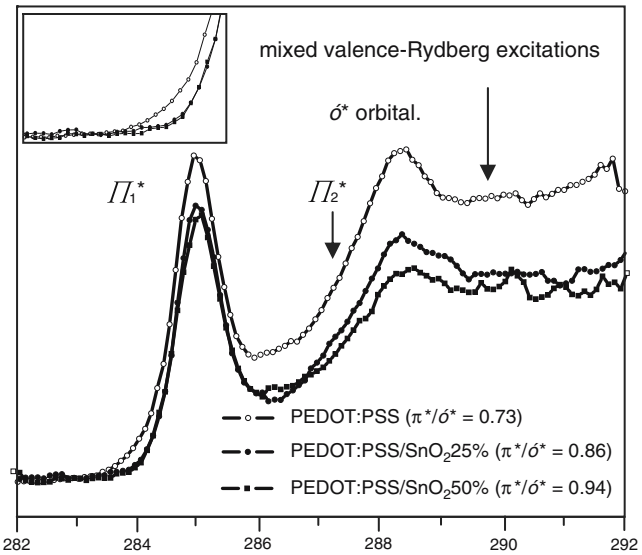

Fig. 4 Normalized C K-edge NEXAFS of PEDOT:PSS, PEDOT:PSS-SnO_2(25%), and PEDOT:PSS-SnO_2 (50%).(inset: enlargement of onset of electron emission)

images derived from AFM tapping mode contains the variation in composition, adhesion, friction, and other properties, including electric property. In Fig. 3a, granular image was observed all over the surface and this could be considered as a particulated PEDOT:PSS polymer complex. However, in case of Fig. 3d, smooth surface image was found and this represents that similar phase is spread out all over the surface uniformly. This morphological change suggested a reorientation of the polymer chain due to the presence of SnO_2 in PEDOT:PSS film. The surface −OH radicals of SnO_2 nanoparticles could be considered to act as a plasticizer in thermal annealing process, like the case of –OH of sorbitol or ethylene glycol [2, 9]. Their electrostatic interaction of PEDOT:PSS was hindered by SnO_2 nanoparticles. Thus, a conductive pathway in PEDOT:PSS increased and high electrical conductivity of the film resulted in. However, in our experiment, the electro-donating oxygen atoms in the SnO_2 may form hydrogen bond with S or C of ethylenedioxythiophene groups in PEDOT and hydroxyl-groups of sulfonic groups in PSS, which weaken the electrostatic interaction between PEDOT cationic chain and PSS chain. Consequently, increase of conductivity can be regarded as an effect of structural change as well as SnO_2 nanoparticles of their own conductivity [10–12]. This structural rearrangement of polymer chains also can be considered from C 1*s* NEXAFS spectra in Fig. 4 and more clearly reflect this structural change with the increase of π–π* transition signal.

In Fig. 4, C 1*s* NEXAFS spectra showed a sharp C 1*s*-π* resonance at 285.2 eV. By the addition of SnO_2 nanoparticle, relative intensity of π* to σ* resonance was increased from 0.73 to 0.86(25%) and 0.94(50%). This also agrees well with AFM images in Fig. 3. The increase in π–π* transition was due to the reorientation of conductive PEDOT chain connectivity in PEDOT:PSS and the stacking with the expanded coil conformation. Furthermore a nanoscale electron transfer at the interface could be expected from the outer oxygen of SnO_2 nanoparticles to the lowest unoccupied molecular orbital state of PEDOT. Besides, at lower energy side of π*-signal, another peak at 283.4 eV was found due to the unoccupied states of bipolaron character [13, 14]. In PEDOT:PSS-SnO_2 composite films, the signal of lower energy side was increased to 283.7 eV (SnO_2-25%) and 283.9 eV (SnO_2-50%). With lower photon energy, electrons emitted at first from SnO_2 nanoparticle (Φ=4.3 eV, Eg=3.6–7 eV [15]) of relatively small work function and trapped in the energy gap of PEDOT:PSS (Φ=5.1 eV http://www.hcstarck.com/pages/497/symposiumelschner6247.pdf). This could be explained by the core-hole screening of electron emitted from SnO_2 nanoparticles, so lower energy side of π_1* resonance increased. The signal at 287.5-289 eV was interpreted as $\sigma^*_{(C\alpha\text{-}S)}$ and $\sigma^*_{(C\text{-}H)}$ resonances [13]. Rydberg-valence mixing which shows low symmetry of the molecules of polymer was also observed in these spectra.

The relative change of work function with SnO_2 nanoparticle addition was measured using secondary electron emission spectra, as show in Fig. 5. The onset of secondary electrons was determined by extrapolating two solid lines from background and straight onset in the spectra. The onset of secondary electron shifts to higher kinetic energy by 0.4 eV in SnO_2 25% addition and 0.5 eV in SnO_2 50% addition, respectively. This means the decrease of carrier concentration and the increase in electron affinity of our composite film near the surface through the n-type SnO_2 addition. The comparison of valence band spectra (Fig. 6)

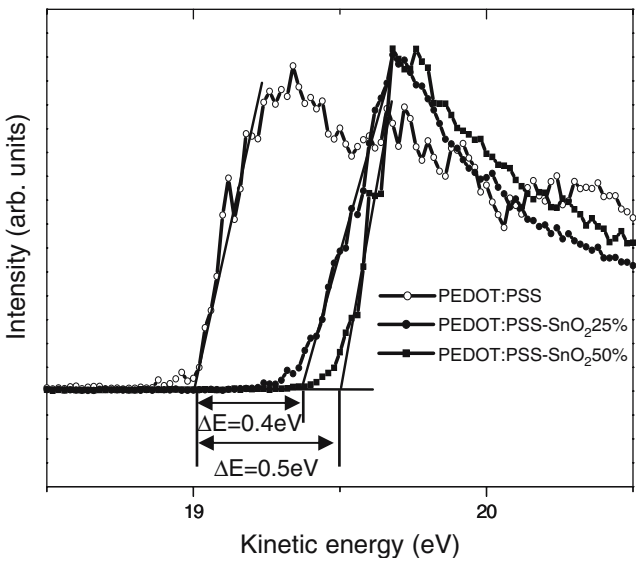

Fig. 5 Secondary electron emission cut off spectra for PEDOT:PSS and PEDOT:PSS-SnO_2 nanocomposite films

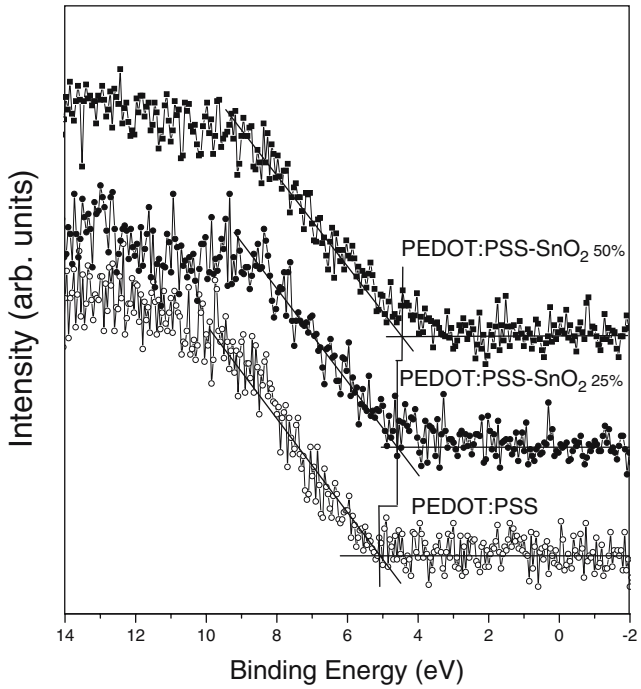

Fig. 6 Relative change of VBM in PEDOT:PSS and PEDOT:PSS-SnO_2 nanocomposite films

shows the relative change in valence band maximum (VBM). The VBM was calibrated with Au 4*f* peak. It is shown that the VBM of PEDOT:PSS surfaces shifted about 0.4 and 0.5 eV to lower bingeing energy with SnO_2 addition of 25 and 50%, respectively, and these results were consistent with the result in C 1*s* NEXAFS analysis. This Fermi level shift corresponds to the increase in PEDOT:PSS upward surface band bending. This could attribute to the formation of the electrostatic incorporation through the SnO_2 nanoparticles with Sn-deficient and O-rich surface and thus VBM increased by electron donation to the VBM of PEDOT:PSS from the SnO_2 nanoparticles with lower work function.

4 Conclusions

We have investigated the influence of SnO_2 nanoparticle on the physical and chemical properties, sheet resistance, morphology, and electronic structure of PEDOT:PSS film. By combining AFM, PES, NEXAFS, and secondary edge emission, the incorporation of SnO_2 nanoparticles induced the changes in morphology, chemical bonding states, and electronic structure. SnO_2 nanoparticles of surface coverage with oxygen and –OH involved in electrostatic interaction of PEDOT:PSS, so that the increased connectivity and more complicated bonding states were observed. In terms of electronic structure, emitted electrons from SnO_2 nanoparticle with n-type and lower work function trapped in the PEDOT:PSS energy band and then increased VBM. Thus it was clearly demonstrated that the work function of PEDOT:PSS could be tuned by the incorporation with SnO_2 nanoparticles.

Acknowledgement The authors would like to acknowledge the financial support from University Research Program supported by Ministry of Information & Communication in Rrepublic of Korea (B1220-0401-0356). The experiments at PAL (4B1) were supported in part by MOST and POSTECH.

References

1. L. Groenendaal, F. Jonas, D. Freitag, H. Pielartzik, J.R. Reynolds, Adv. Mater. **12**, 481 (2000)
2. W.H. Kim, A.J. Mäkinen, N. Nikolov, R. Shashidhar, H. Kim, Z. H. Kafafi, Appl. Phys. Lett. **80**, 3844 (2002)
3. S.K.M. Jönsson, J. Birgerson, X. Crispin, G. Greczynski, W. Osikowicz, A.W. Denier van der Gon, W.R. Salaneck, M. Fahlman, Synth. Met. **139**, 1 (2003)
4. X. Crispin, S. Marciniak, W. Osikowicz, G. Zotti, A.W. Denier. van der Gon, F. Louwet, M. Fahlman, L. Groenendaal, F. De Schryver, WR Salaneck, J. Polym. Sci., B **41**, 2561 (2003)
5. F. Gu, S.F. Wang, C.F. Song, M.K. Lü, Y.X. Qi, G.J. Zhou, D. Xu, D.R.Yuan, Chem. Phys. Lett. **372**, 451 (2003)
6. B.D. Cullity, *Elements of X-ray Diffraction*, 2nd edn. (Addison-Wesley Pub Co., 1978), p. 102
7. D. Schmeißer, O. Böhme, A. Yfantis, T. Heller, D. R. Batchelor, I. Lundstrom, A.L. Spetz, Phys. Rev. Lett. **83**, 380 (1999)
8. G. Greczynski, Th. Kugler, M. Keil, W. Osikowicz, M. Fahlman, W.R. Salaneck, J. Electron Spec. Rel. Phenom. **121**, 1 (2001)
9. M.P. de Jong, A.W. Denier van der Gon, X. Crispin, W. Osikowicz, W.R. Salaneck, L. Groenendaal, J. Chem. Phys. **118**, 6495 (2003)
10. J. Ouyang, C.W. Chu, F.C. Chen, Q. Xu, Y. Yang, Adv. Mater. **15**, 203 (2005)
11. A.G. MacDiarmid, A.J. Epstein, Synth. Met. **65**, 103 (1994)
12. J. Ouyang, Q. Xu, C.W. Chu, Y. Yang, G. Li, J. Shinar, Polymer **45**, 8443 (2004)
13. S. Tepavcevic, A.T. Wroble, M. Bissen, D.J. Wallace, Y. Choi, L. Hanley, J. Phys. Chem., B **109**, 7134 (2005)
14. A.L. Dawar, J.C. Joshi, J. Mater. Sci. **19**, 1 (1984)
15. A.C. Ariasa, L.S. Romanb, T. Kuglerb, R. Tonioloc, M.S. Meruviac, I.S. Hummelgenc, Thin Solid Films, **371**, 201 (2000).